Supplementary material

Optimization of zoned irrigation to balance groundwater sustainability and crop yield under future irrigation source replacement scenarios

Miao Jing[1,2], Chunhui Lu[2,3,4*], Yushan Wang[5], Jina Yin[2,3], Jin Liu[1,2], Yu Ye[6,2]

1. School of Earth Science and Engineering, Hohai University, Nanjing 210098, China, 2. The National Key Laboratory of Water Disaster Prevention, Hohai University, Nanjing 210098, China, 3. Yangtze Institute for Conservation and Development, Hohai University, Nanjing 210098, China, 4. College of Hydrology and Water Resources, Hohai University, Nanjing 210098, China, 5. Center for Hydrogeology and Environmental Geology Survey, China Geological Survey, Baoding 300309, China, 6. College of Water Conservancy and Hydropower Engineering, Hohai University, Nanjing 210098, China

*Corresponding author: Chunhui Lu, clu@hhu.edu.cn

Contents

Text S1–S4

Fig. S1–S3

Text S1 describes the lower- and upper-limit relationships between irrigation quota and winter wheat yield change.

Text S2 provides a detailed description of the rainfall forecasting method—SARIMA.

Text S3 describes the historical evolution of water-balance components and groundwater anomalies in Cangzhou during 2009–2020.

Text S4 describes the regional water-balance and groundwater-extraction projection workflow used for the 2021–2040 groundwater scenarios.

Fig. S1 shows projected future water demand under the control scenario and three socioeconomic scenarios.

Fig. S2 shows the projected monthly precipitation for Cangzhou from 2021 to 2040.

Fig. S3 shows the historical groundwater-budget components and cumulative storage anomaly in Cangzhou during 2009–2020.

Text S1

Lower- and upper-limit winter wheat yield responses

The relationship between winter wheat yield change and irrigation quota for the lower limit and the upper limit scenarios are:

$$\Delta Y = -7.327 \times 10^{-6} \cdot I^2 + 0.002946 \cdot I - 0.3316 \quad \text{(S1)}$$

and

$$\Delta Y = -3.883 \times 10^{-6} \cdot I^2 + 0.002327 \cdot I - 0.2627, \quad (S2)$$

respectively.

Text S2

Rainfall forecasting using SARIMA

To evaluate trade-offs between groundwater sustainability and crop yield under future ISR scenarios, we forecasted monthly precipitation for 2021–2040 utilizing a historical baseline from 1961 to 2020. A Seasonal Autoregressive Integrated Moving Average (SARIMA) model was selected as it effectively captures both non-stationary long-term trends and distinct 12-month cyclical patterns. To prevent the mean-converging smoothing typical of long-term statistical forecasts and to rigorously test the *irrigmoo* optimization framework, we introduced a stochastic noise term. This coupling preserves realistic climate variability, accurately simulating the extreme hydrological events (e.g., severe droughts) that fundamentally drive agricultural groundwater demand.

The forecasting framework was implemented through three primary stages:

Data Integration: A continuous monthly precipitation time series (Y_t) from 1961 to 2020 was constructed by aggregating daily historical records (1961–2013) into monthly totals, and splicing them with recent monthly-averaged daily records (2009–2020) appropriately adjusted by the days per month.

Model Configuration: The time series was fitted to a SARIMA $(p, d, q) \times (\mathrm{P}, \mathrm{D}, \mathrm{Q})_{\mathrm{s}}$ model. Based on historical autocorrelation functions (ACF/PACF), non-seasonal parameters (p, d, q) were set to (1, 1, 1), applying first-order autoregression, non-seasonal differencing for stationarity, and a first-order moving average. To account for the annual climatic cycle, seasonal parameters (P, D, Q) were assigned as (1, 1, 1) with a periodicity of $s = 12$. Parameters were optimized using Maximum Likelihood Estimation (MLE).

Stochastic Forecasting: The calibrated model generated a baseline prediction mean ($\hat{Y}_t$) for the 240-month forecast horizon (2021–2040). To simulate natural meteorological perturbations, the final forecasted precipitation, $P_forecast(t)$, was defined by superimposing a white noise term:

$$P_{forecast}(t) = max\left(0, \hat{Y}_t + \varepsilon_t\right)$$

Text S3

Historical hydrologic components and groundwater anomaly between 2009–2020

The inflow anomalies (Fig. S3a) exhibit pronounced seasonal fluctuations, with peaks primarily driven by recharge inputs, supplemented by lateral inflow, indicating strong climatic and hydrological control on groundwater replenishment. In contrast, the outflow anomalies (Fig. S3b) are dominated by pumping from wells, showing sharp and recurrent peaks that reflect intensive groundwater extraction during irrigation periods, while lateral outflow remains relatively small and stable.

The combined effect of these inflow and outflow dynamics is reflected in the groundwater storage anomalies (Fig. S3c), which display clear seasonal drawdown–recovery cycles. Periods of negative storage anomalies correspond to months when pumping exceeds recharge, whereas partial recovery occurs during intervals of enhanced recharge and reduced extraction. Specifically, storage generally declines toward the mid-2010s, indicating that pumping and other discharge terms exceeded recharge and lateral inflow over this period. After 2015, the cumulative anomaly shows partial recovery, suggesting a weakening of the historical depletion tendency. This transition is consistent with reported groundwater stabilization in parts of the North China Plain following increased water-management interventions and IBWD. Overall, the figure highlights that groundwater storage variations are primarily controlled by the imbalance between recharge-driven inflows and pumping-dominated outflows, underscoring the critical role of irrigation practices in governing the seasonal and interannual dynamics of confined groundwater storage in the study area.

Text S4

Regional water-balance and groundwater-extraction projection workflow

Within the *irrigmoo* simulation and optimization framework, the regional water supply and demand balance for the Cangzhou area is governed by the principle that the total annual water demand ($\mathrm{D_{tot}}$) must be met by a combination of local surface water ($\mathrm{S_{sw}}$), groundwater extraction ($\mathrm{S_{gw}}$), water diverted from the SNWD project ($\mathrm{S_{IBWD}}$), and water diverted from other sources ($\mathrm{S_{dv0}}$, i.e., primarily from Yellow River). Accordingly, the fundamental water balance equation is expressed as:

$$\mathrm{D_{tot}} = \mathrm{S_{sw}} + \mathrm{S_{gw}} + \mathrm{S_{IBWD}} + \mathrm{S_{dv0}} \quad \text{(S3)}$$

Our study explicitly considers three SSPs and the baseline scenario to project the future water demand, $\mathrm{D_{tot}}$, based on prior studies (Long et al., 2025; Yang et al., 2022). Nevertheless, the main objective of our study is quantifying the influence of different target-driven irrigation on the future GWL dynamics. Therefore, we calculate the averaged D_{tot} of four socioeconomic scenarios as the projected water demand. Details of the water-demand projection can be found in Fig. S1.

Local surface water availability in the study area is highly sensitive to climate variability. S_{sw} is projected based on its historically established relationship with annual precipitation (P). A linear regression model, calibrated using available historical data, is employed to estimate future surface water supply (Li et al., 2025):

$$S_{sw} = 0.00476 \times P + 0.22647 \quad \text{(S4)}$$

For the future projection period (2021–2040), the annual precipitation variable (P) is dynamically supplied by the Stochastic SARIMA model forecasts, ensuring that the optimization framework accounts for realistic interannual climate fluctuations and extreme hydrological events. The detailed forecast of the annual precipitation can be found in Text S2 and Fig. S2.

Based on statistical books and reports, the diverted volume from the other surface-water sources (e.g., Yellow River), S_{dv0}, is approximately 3.36×10^8 m^3/yr, which is assumed to remain unchanged for the future projection.

The target-driven modifications are exerted on S_{gw} and S_{IBWD}. Specifically, S_{IBWD} is determined by the four prior ISR scenarios. The groundwater resources are planned as backup water reserves. Accordingly, S_{gw} is calculated following a two-step workflow: (1) The baseline value S_{gw} is calculated using Eq. (S3) after determining all water demands and water uses, (2) S_{gw} is then modified using the optimized zoned irrigations by substituting the replaced volume in four ISR scenarios. This two-step workflow guarantees that the potential of water diversion is fully released to fulfill the demand for winter wheat irrigation.

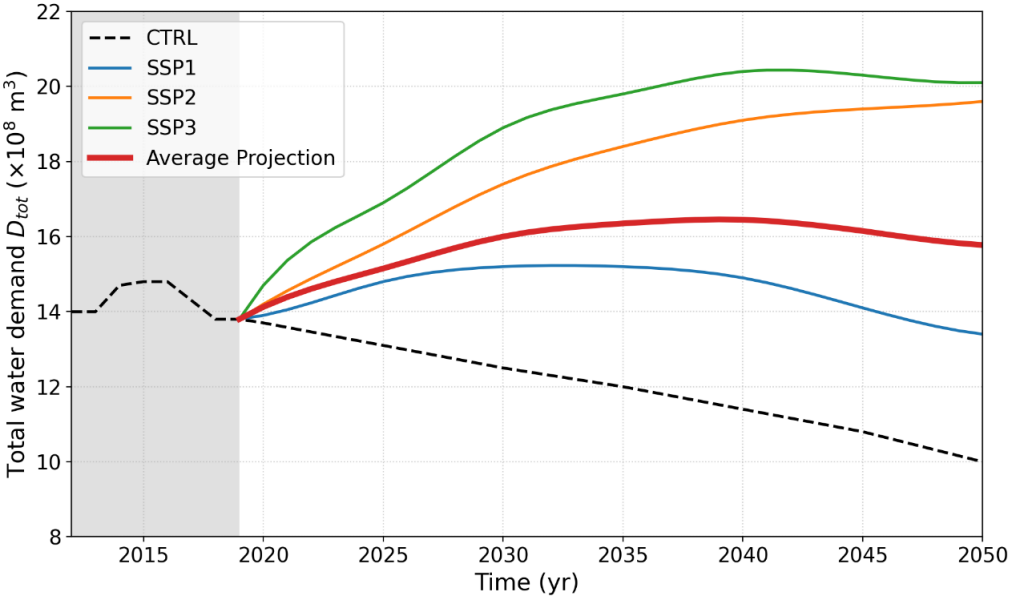


Fig. S1. Projected total water demand ($\boldsymbol{D_{tot}}$) in Cangzhou under socioeconomic development scenarios from 2012 to 2050. The dashed black line represents the control scenario (CTRL), while the blue, orange, and green lines represent SSP1, SSP2, and SSP3, respectively. The thick red line indicates the average projection used in the groundwater-level projection framework. The gray shaded area denotes the historical reference period from 2012 to 2019. Water demand is expressed in 10^8 m^3.

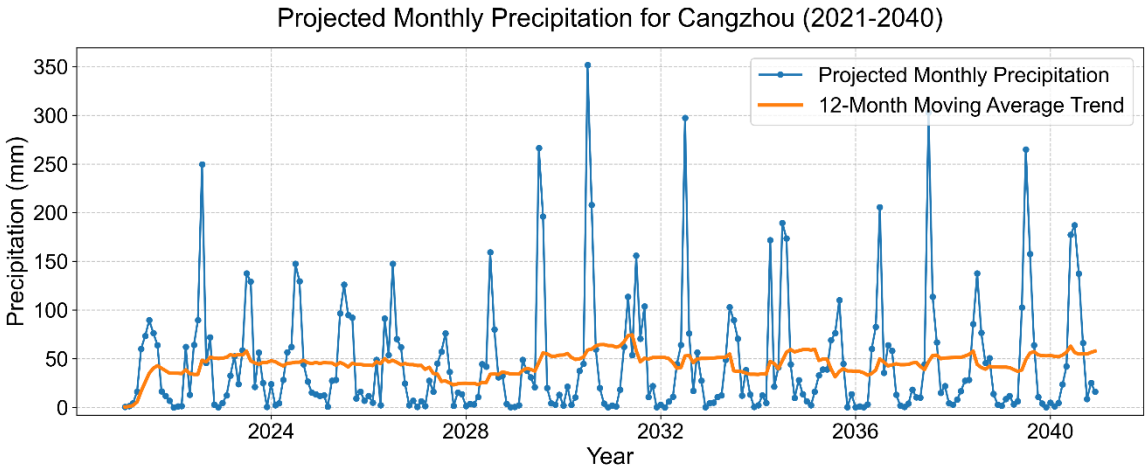


Fig. S2. Projected monthly precipitation for Cangzhou from 2021 to 2040. Blue markers and lines show projected monthly precipitation totals generated from the historical precipitation record, and the orange line shows the 12-month moving average trend. The x-axis is extended to start in 2009 for consistency with the model simulation period.

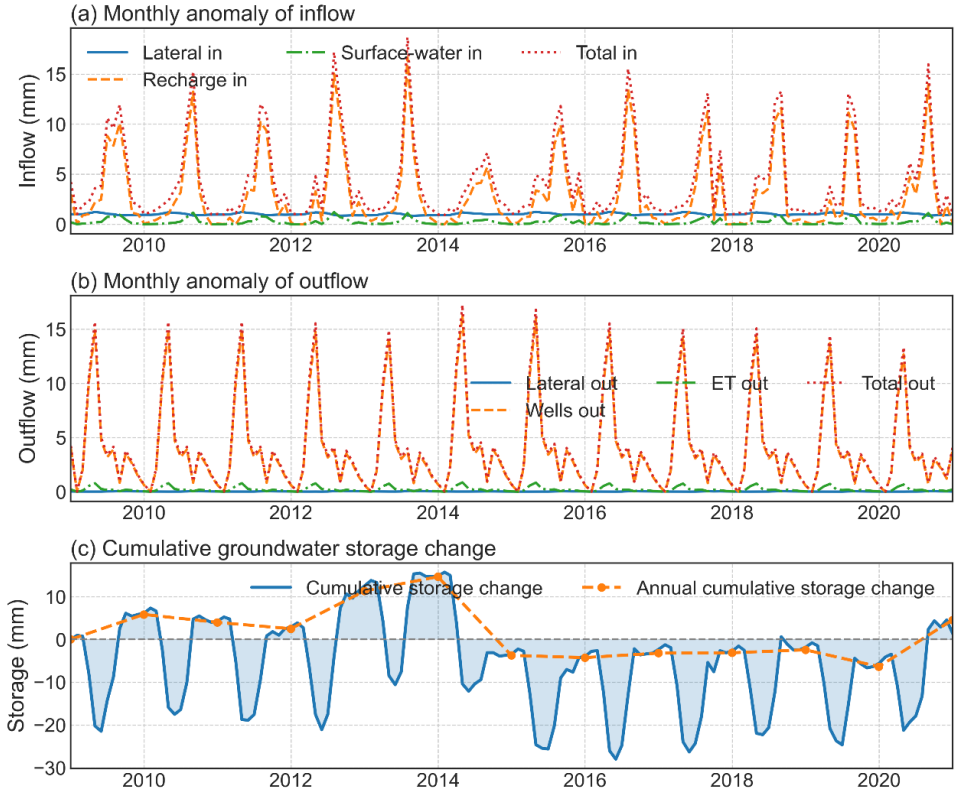


Fig. S3. Historical groundwater-budget components and cumulative storage anomaly in Cangzhou during 2009–2020. All fluxes are converted to equivalent water depth over the model domain. Panel (c) shows the cumulative groundwater storage anomaly, with annual values superimposed to emphasize interannual storage variability.

115

References

Li, H., Guo, Z., Chen, K., Zhan, Y., Wang, Y., Ding, C., Lu, C., and Zheng, C.: Modeling Land Subsidence Under Future Water Stress: The Influence of Groundwater Exploitation, Climate Change, and Inter-Basin Water Diversion, Water Resour. Res., 61, e2025WR041105, https://doi.org/10.1029/2025wr041105, 2025.

120 Long, D., Xu, Y., Cui, Y., Cui, Y., Butler, J. J., Jr., Dong, L., Wang, L., Liu, D., Wada, Y., Hu, L., Bai, G., Li, B., Wang, S., Nong, X., Cai, Y., Cheng, C., Mu, Y., Qiao, Y., Wang, J., Wang, H., and Scanlon, B. R.: Unprecedented large-scale aquifer recovery through human intervention, Nat. Commun., 16, 7296, https://doi.org/10.1038/s41467-025-62719-5, 2025.

Yang, W., Long, D., Scanlon, B. R., Burek, P., Zhang, C., Han, Z., Butler, J. J., Jr., Pan, Y., Lei, X., and Wada, Y.: Human Intervention Will Stabilize Groundwater Storage Across the North China Plain, Water Resour. Res., 58, e2021WR030884,

125 https://doi.org/10.1029/2021wr030884, 2022.